Arabian Journal of Chemistry (2019) **12**, 262–271

King Saud University

Arabian Journal of Chemistry

www.ksu.edu.sa
www.sciencedirect.com

ORIGINAL ARTICLE

Biosilica-nanogold composite: Easy-to-prepare catalyst for soman degradation

Veronika Holišová [a,*], Martin Urban [b], Marek Kolenčík [c], Yvonne Němcová [d], Adam Schröfel [e], Pavlína Peikertová [f], Jiří Slabotinský [b], Gabriela Kratošová [a]

[a] *Nanotechnology Centre, VŠB – Technical University of Ostrava, 17. listopadu 15/2172, 708 33 Ostrava – Poruba, Czech Republic*
[b] *National Institute for Nuclear, Biological and Chemical Protection, v.v.i., Kamenná 71, 262 31 Milín, Czech Republic*
[c] *Department of Soil Science, Slovak University of Agriculture in Nitra, Tr. A. Hlinku 2, 949 76 Nitra, Slovakia*
[d] *Faculty of Science, Charles University, Benátská 433/2, 128 43 Prague, Czech Republic*
[e] *Faculty of Science, Charles University, Albertov 6, Prague 2, Czech Republic*
[f] *IT4 Innovations Centre of Excellence, Nanotechnology Centre, VŠB – Technical University of Ostrava, 17. listopadu 15/2172, 708 33 Ostrava – Poruba, Czech Republic*

Received 14 March 2017; accepted 8 August 2017
Available online 18 August 2017

KEYWORDS

Biosynthesis;
Biosilica;
Nanogold;
Catalysis;
Soman

Abstract A very fast single-step biosynthesis of gold nanoparticles (AuNPs) using algal cells of *Mallomonas kalinae* (MK) is introduced. The average particle size of crystalline AuNPs was approximately 10 nm. Subsequently, the catalytic activity of two systems – MK-biosilica scales and MK-biosilica scales with AuNPs – was compared with a control hydrolysis of soman (GD) performed in demineralized water. The kinetics of GD degradation was studied using a gas chromatography with mass detector (GC–MS) and solid-phase microextraction. The residual content of GD was 3.8% and 3.5% for both initial concentrations of GD (68 μg mL^{-1} and 340 μg mL^{-1}, respectively) after 48 h of testing when nanogold was used as a catalyst. Experimental results confirmed the catalytic activity of biosynthesized AuNPs, as well as the role of biosilica itself in the degradation of GD.

1. Introduction

Chemical warfare agents (CWA) pose an almost inconceivable threat to human health and the environment. In response to these threats, the research community has been trying for a long time to find effective and safe ways of CWA decontamination. Although there is an international agreement "Convention on the Prohibition of the Development, Production, Stockpiling and Use of Chemical Weapons and on their Destruction" (Organization for the Prohibition of Chemical Weapons, 2014), CWA are still produced and developed for

* Corresponding author.
E-mail address: Veronika.Holisova.st@vsb.cz (V. Holišová).
Peer review under responsibility of King Saud University.

Production and hosting by Elsevier

http://dx.doi.org/10.1016/j.arabjc.2017.08.003
1878-5352

military use. CWA can be divided into several groups, e.g. blistering, choking, blood and nerve agents (NA); NA can be further classified into G- and V-series agents. Tabun (GA), sarin (GB), soman (GD) and cyclosarin (GF) belong to the G-series agents. The V-series agents comprise VX and R-VX compounds (Kim et al., 2011). Soman (O-Pinacolyl methylphosphonofluoridate) is the most effective G-type nerve agent. The median lethal dose for a human is in the range from 2 to 10 mg. Soman is sparingly soluble in water (21 g L^{-1} at 20 °C) but still sufficient for lethal poisoning (Gupta, 2009; Romano and Salem, 2008). The principle of the toxic effect of NA is in its ability to irreversibly inhibit the enzyme acetylcholinesterase, which is responsible for the degradation of acetylcholine. When acetylcholine does not degrade, it accumulates and triggers a crisis of the nerve system, which leads to poisoning. Certain methods and techniques to degrade NA into less toxic, less persistent or non-toxic substances have already been developed (Kim et al., 2011). According to the toxicological study, the methylphosphonic acid (MPA) is the final degradation product of soman and is considered as practically non-toxic (Kim et al., 2011). After the hydrolysis of NA, the by-products of degradation may be utilized as potential nutrients acceptable in the life cycles of some aquatic and soil organisms (Karpouzas and Singh, 2006). Hydrolysis, oxidation, nucleophilic and electrophilic substitution (Kim et al., 2011) or photochemical reactions (Komano et al., 2013) represent the most common degradation mechanisms.

Several studies focused on the degradation of CWA and their simulants using different kinds of nanomaterials have also been introduced; materials applied were modified TiO_2 (Alvaro et al., 2010), zirconium-doped nano-dispersed oxides (Němec, 2010) or Fe-oxohydroxides (Zboril et al., 2012). Their high catalytic activity is directly connected with desired properties such as nano-sized morphology (a combination of several quantum effects), hybrid layering (electron capturing), the range of band-gap energy (Cuenya, 2010), and also generation of radicals and electron holes (Alvaro et al., 2010; Komano et al., 2013). The combination of these characteristics leads to the disruption of active bonds and groups of atoms in the organophosphate molecule. In this respect, nanogold is one of the most catalytically active elements due to its remarkable thermodynamic stability and inertness (Corti, 2010; Khan et al., 2014). This excellent catalytic activity of AuNPs can be utilized for purposes other than the degradation of NA (Schröfel et al., 2014).

Catalytically active nanomaterials have been traditionally prepared by physical or chemical methods requiring high temperatures (Zboril et al., 2012), long-lasting preparation protocols (Janoš et al., 2015) or complicated experimental equipment along with high consumption of energy (Alvaro et al., 2010). Moreover, hazardous toxic chemicals posing various biological risks are often used (Ahmed et al., 2016). The biosynthesis of nanoparticles offers an inexpensive, non-toxic and environmentally friendly method of preparation. The main advantage of biosynthesis opposed to abiotic methods is the ability to form nanoparticles without a significant aggregation and need for subsequent stabilization (Ahmed et al., 2016; Manivasagan and Kim, 2015). Nowadays, different kinds of bacteria (Sweeney et al., 2004), micro-fungi (Vágó et al., 2016), plant extract (Gopinath et al., 2019; Kolenčík et al., 2014) as well as algae (Mubarak Ali et al., 2013; Schröfel et al., 2011) may be employed for the biosynthesis of nanoparticles.

The aim of the presented work is to highlight the possibility of preparation of new catalytically active composite nanomaterials using eco-friendly biosynthesis protocols, in our case by use of *Mallomonas kalinae* (MK) silica cells. Our designed biohybrid material is composed of 3 D hierarchal biosilica with pores in nano-to-micrometer scale on its surface, external nature-related functional polymeric substances and anchored AuNPs. Obviously, such designing of new catalysts represents a state-of-the-art interdisciplinary approach with great engagement of biotechnology.

2. Experimental

2.1. Cultivation and treatment of MK

MK cells (Fig. 1) were obtained from the Culture Collection of Algae of the Charles University in Prague, Department of Botany, Czech Republic (strain B 601). The experimental culture was grown in 0.5 L Erlenmeyer flasks containing a DY-V medium (Andersen et al., 1997) covered with aluminum foil into which 1 mL of water glass ($Na_2SiO_3 \cdot 5H_2O$) was added every 4 days. Cells were inoculated into the medium under aseptic conditions in a flow-box (BHL 65). Cells of MK were incubated for 30 days under constant illumination at 24 °C (15 µmol m^{-2} s^{-1}, 18 W fluorescent lamp Philips TDL 18 W/33).

MK cells were decanted at the end of the exponential growth phase and the biomass was concentrated by centrifugation. The centrifugation was performed with a Sigma 2–16 PK for 5 min at 4 °C and 3612 rpm using swing-out rotors. The supernatant was removed and settled cells were collected in a reservoir bottle.

2.2. Biosynthesis of AuNPs

A stock culture of 1 L (concentrated MK cells; pH 6.5) was prepared by the aforementioned cultivation and centrifugation. 750 mL of the stock culture was mixed with 7.5 mL of 0.1 M $HAuCl_4$ (Sigma-Aldrich, USA) in temperate laboratory conditions. After the biosynthesis, the resulting pH of the

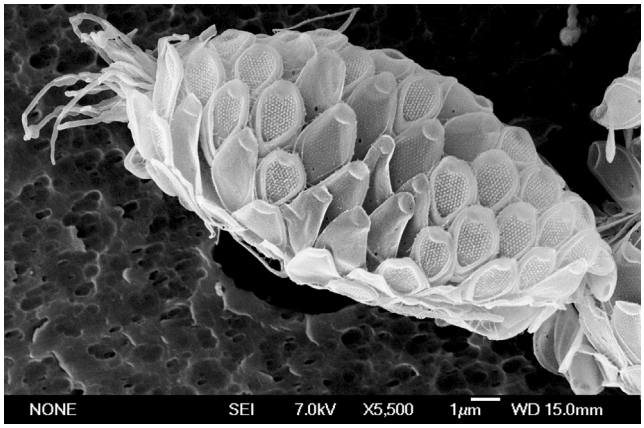

Fig. 1 *Mallomonas kalinae* cell covered with overlapping silica scales.

mixture containing AuNPs and cell debris reached the value of pH = 3.4. The remainder of the concentrated cell suspension was stored for control experiments.

2.3. Microscopic characterization and size distribution of AuNPs

Pure cells of MK were observed by a scanning electron microscope (JEOL JSM-7401F) at The Czech Academy of Sciences in České Budějovice, Czech Republic. The change of color of the cell suspension after mixing with gold precursor was observed both visually and using light microscope (OLYMPUS BX51) at the Department of Botany of Charles University in Prague. A reaction mixture of AuNPs with MK cell debris was further characterized by a transmission electron microscope (FEI Tecnai Sphera G2) operated with accelerating voltage 200 kV at the Medical Faculty of Charles University in Prague, Czech Republic.

The evaluation of size distribution of AuNPs was performed by JMicroVision software (http://www.jmicrovision.com). At least 200 AuNPs from TEM micrographs per sample underwent the image analysis.

2.4. Spectroscopic characterization

The characteristic absorption of AuNPs was measured using the ultraviolet–visible spectrophotometer (UV–Vis) Evolution 60 S (Thermo Fisher Scientific, USA) with a unit step of 0.5 nm in the wavelength range of 300–800 nm. A Fourier transform infrared spectrophotometer (FTIR) Nicolet 6700 FT-IR (Thermo Nicolet, Waltham, USA) was used to characterize functional groups and biomolecules of MK cells and their changes before and after the biosynthesis. The FTIR spectrometer functions according to the Attenuated Total Reflectance (ATR) technique using a diamond crystal. The spectra were measured in the range of 400–4000 cm^{-1}. XRD patterns were recorded under CoKα irradiation (λ = 1.789 Å) using the Bruker D8 Advance diffractometer (Bruker AXS, Billerica, USA) equipped with a fast position sensitive detector VÅNTEC 1. EVA software was used for the evaluation of X-ray patterns. The content of AuNPs in biosilica-based nanocomposite was determined by atomic emission spectrometry with inductively coupled plasma (AES-ICP) Ciros Vision (SPECTRO Analytical Instruments Inc., Kleve, Germany).

2.5. Computer data processing

The Visual Minteq (VM) program 3.1 (http://vminteq.lwr.kth.se) is an equilibrium speciation modeling tool that can be used to calculate the equilibrium composition of dilute aqueous solutions in laboratory testing or in natural aqueous systems. The model is useful for calculating the equilibrium mass distribution among dissolved or adsorbed species, and multiple solid phases under a variety of conditions including a gas phase with constant partial pressures (Zhang et al., 2008).

The soluble products in the DY-V medium were evaluated using VM prior to the cultivation of MK. Geochemical speciation of the DY-V medium was implied at pH 7. Input data were obtained from the total dissolved concentrations of cations Ca^{2+}, Mg^{2+}, Na^{+}, K^{+}, Fe^{3+}, anions Cl^{-}, SO_4^{2-}, CO_3^{2-}, NO_3^{-}, $EDTA^{4-}$, and H_4SiO_4. The data processed may help to interpret the possible background of GD degradation.

2.6. Soman degradation

Analyses of GD degradation were performed at the National Institute for Nuclear, Biological and Chemical Protection in Kamenná, Czech Republic. Agilent's Gas Chromatography systems (Agilent 7890A, Agilent Technologies, USA) equipped with solid phase microextraction and HP-5 MS silica column (30 m length, 0.25 mm inner diameter, 0.25 μm film thickness) was used to monitor the soman degradation. For solid phase microextraction, a 65-μm fiber PDMS/DVB (polydimethylsiloxane/divinylbenzene), Stableflex Supelco was used. Fiber sorption and desorption time was 300 s at 250 °C. Agitator at 500 rpm for 180 s was used to homogenize matrices (Table 1). The GC temperature program was as follows: 45 °C/min, 80 °C/min, and finally 280 °C/5 min. Helium (99.9% purity) was used as the carrier gas with the flow rate of 1 mL min^{-1}. Degradation products were detected and determined using mass spectroscopy (Agilent 5975 C inert XL) and software MSD ChemStation (E.02.02.1431) with a library of spectra NIST 08.

Two distinct initial concentrations and volumes of GD (purity > 95%) were tested in the experiments of GD hydrolysis: 68 μg $mL^{-1}$of GD (1 μl added) and 340 μg.mL^{-1} of GD (5 μl). Soman was mixed with 15 mL of (i) demineralized water in the control experiment, (ii) a solution containing only pure MK cells, (iii) a solution with AuNPs and cell debris of MK. Thus, six different matrices were tested (see Table 1) and their dosing into the column was carried out at hourly intervals for 48 h.

All reactions were fitted using pseudo-first order kinetics and the rate constant (k) was calculated by the Eq. (1) in the following form:

$$c = c_0 \times e^{-kt}, \quad (1)$$

where c and c_0 describe the content of soman (%) at a given time t and at time zero, respectively and t is reaction time (h).

3. Results and discussion

3.1. Characterization of biosilica-nanogold composite

The color change of the cell suspension after the addition of gold precursor was observed visually (Fig. 2). Nanoparticles

Table 1 The composition of tested matrices (M1–M6): 15 mL of particular solutions (demineralized water, pure MK cells or AuNPs/MK) was mixed with GD of two different concentrations (c_{GD} = 68 μg mL^{-1} and 340 μg mL^{-1}) and volumes (1 or 5 μl) to give six different reaction mixtures.

M1	$_{DEMI}H_2O$	V_{GD} = 1 μl
M2	pure MK cells	c_{GD} = 68 μg mL^{-1}
M3	AuNPs and MK debris	
M4	$_{DEMI}H_2O$	V_{GD} = 5 μl
M5	pure MK cells	c_{GD} = 340 μg mL^{-1}
M6	AuNPs and MK debris	

started to form immediately after the MK cells came in contact with the gold precursor solution, which was easily observable. The solution became purple within a few minutes, confirming the great reduction potential of the biomass used in the AuNPs biosynthesis, and forming of biosilica-nanogold functional composite.

Changes before and after the bioreduction of Au^{3+} ions were observed by UV–Vis spectroscopy. UV–Vis analysis confirmed the presence of AuNPs (Fig. 3) in biosilica-nanogold suspension. The spectrum shows a typical absorption peak around 543 nm, which corresponds with the AuNPs plasmon resonance (Vágó et al., 2016; Zhang et al., 2016). In the concentrated MK cell suspension several peaks were observed corresponding to a more diverse composition of this environment. The peaks around 406 and 665 nm correspond to the presence of chlorophyll *a* (Makarska-Bialokoz and Kaczor, 2014).

The crystalline structure of biosynthesized AuNPs was confirmed by XRD pattern analysis. The XRD pattern in Fig. 4 shows three characteristic diffraction peaks at 2 theta values 45°, 52° and 77° corresponding to (1 1 1), (2 0 0) and (2 2 0) planes of cubic crystal structure of gold.

TEM micrographs revealed AuNPs localized at two different locations. AuNPs were situated directly on the porous surface of biosilica scales (Fig.5a) and in the external polymeric substances (EPS) outside the cells (Fig.5b). Particle size distribution histograms were created for the most common spherical AuNPs on the biosilica surface and in the EPS (Fig. 5). The average size of AuNPs was different on the biosilica scales (around 7 nm) and in the surrounding area (around 14 nm).

Various morphological types of biosynthesized AuNPs are presented in the Fig. 6. Spherical nanoparticles are most prone to aggregation. A sticking coefficient calculated was in the range of 10% to 50%. On the other hand, triangular and rod-shaped nanoparticles usually occur in isolation. They aggregate mostly with spherical nanoparticles (sticking coefficient of 10%) which are situated at the edges. AuNPs formed at least three morphological types (Fig. 6). The most dominant

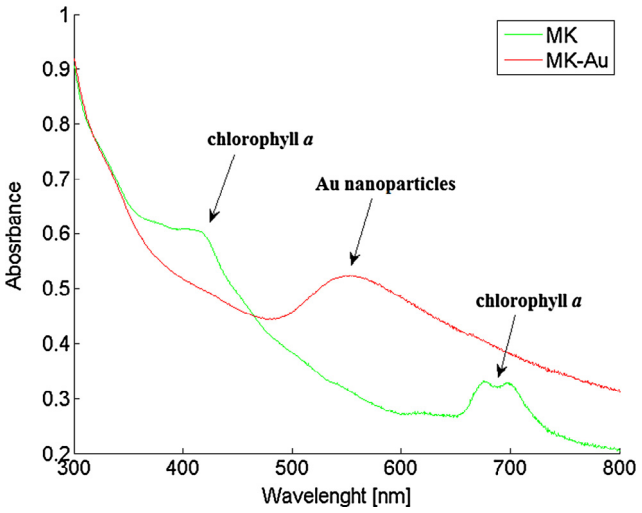

Fig. 3 UV–Vis spectra: green line – concentrated MK cell suspension; red line – MK cell suspension with biosynthesized AuNPs.

were spherical nanoparticles, which had approximately the same size vertically and horizontally. Triangular crystals, which created equilateral triangles with a flat surface, were also present. An additional morphological type observed on the TEM micrographs was rod-shaped with a vertical to horizontal ratio of 1:3 to 1:7.

The most dominant component of the suspension containing AuNPs and MK cell debris was the biosiliceous matrix of algae serving as the support for AuNPs. The surface of MK scales is composed of amorphous and porous SiO_2 (Jablonski, 1990). The pores on the MK scales are uniformly distributed and represent a rhombohedral and extremely symmetric network (Fig. 7). The relative constant distance between the pores measured vertically and horizontally was from 90 to

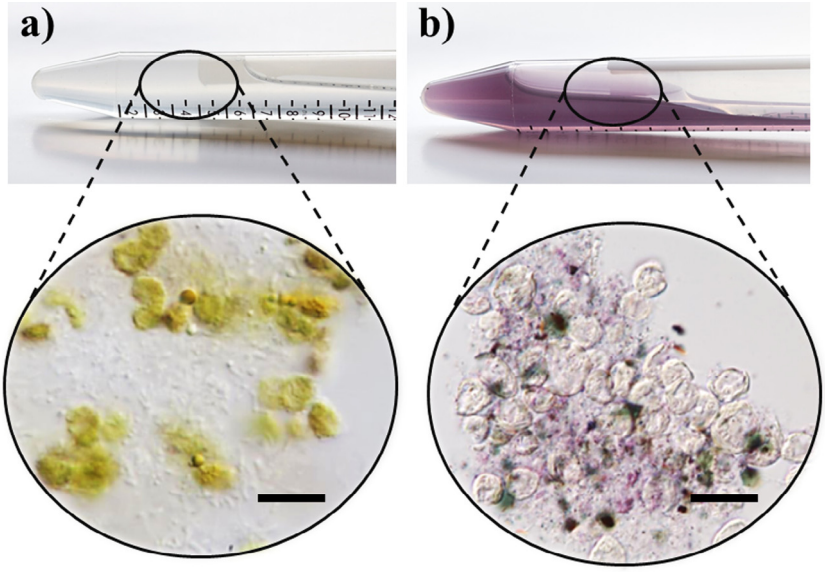

Fig. 2 Photo documentation of Falcon test tubes and light microscopy images: (a) *Mallomonas kalinae* (MK) cell suspension before experiment and (b) after the biosynthesis treatment with observable color changes (purple color) with determined gold nanoparticles (scale bar 10 μm).

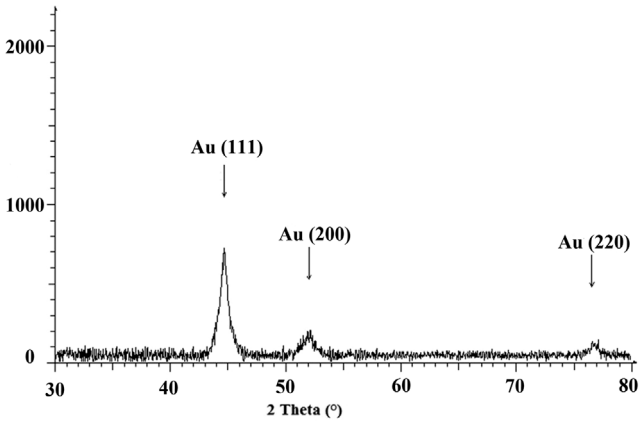

Fig. 4 X-ray diffraction pattern of AuNPs.

97 nm. The pore size was from 41 to 48 nm. Thus, it was creating a functional hybrid material (bionanocomposite) applicable in the catalytic hydrolysis of GD.

3.2. Biosilica-nanogold composite formation

The possible mechanism of Au ions bioreduction into AuNPs in the present of MK was studied using FTIR spectroscopy. A FTIR analysis was performed to detect changes in the functional groups before and after the biosynthesis. Two FTIR spectra were compared: (1) the spectrum of pure MK and (2) MK with AuNPs (Fig. 8).

In the pure MK, spectrum bands 2949, 2923, 2871, and 2852 cm^{-1} corresponded to the presence of —CH_3 and —CH_2 symmetric and asymmetric vibrations. The band at 1453 cm^{-1} indicated a deformation vibration of C—H bonds and the band at 1409 cm^{-1} represented a vibration of C—O bond in a carbonyl group. The band at position 1733 cm^{-1} corresponded to the occurrence of C═O bond in esters or amino acids. A wide band around 3272 cm^{-1} corresponded to the stretching vibrations of O—H bonds in the sample, and a deformation vibration of the O-H bonds should have been present at 1630 cm^{-1} (Oliveira et al., 2014). However, there was overlapping with the vibrations related to the presence of proteins in this area. Proteins in the sample were proven by bands at 1632 and 1540 cm^{-1} (structure of amid I. and amid II.). Proteins may form a stabilizing coat on AuNPs to prevent their aggregation (Abdel-Raouf et al., 2017). The most intense band at 1045 cm^{-1} with the shoulder at 1155 cm^{-1} corresponds to the Si—O—Si vibration of biosilica of MK cells. In addition, other bands (795, 698 and 456 cm^{-1}) corresponded to the presence of different Si-O biosilica vibrations as well.

There were a few differences in the spectrum of MK–Au. The intensity of this spectrum was a little bit less intensive than the spectrum of pure MK cells, probably due to the presence of gold in the sample, which itself is not active in the mid-infrared

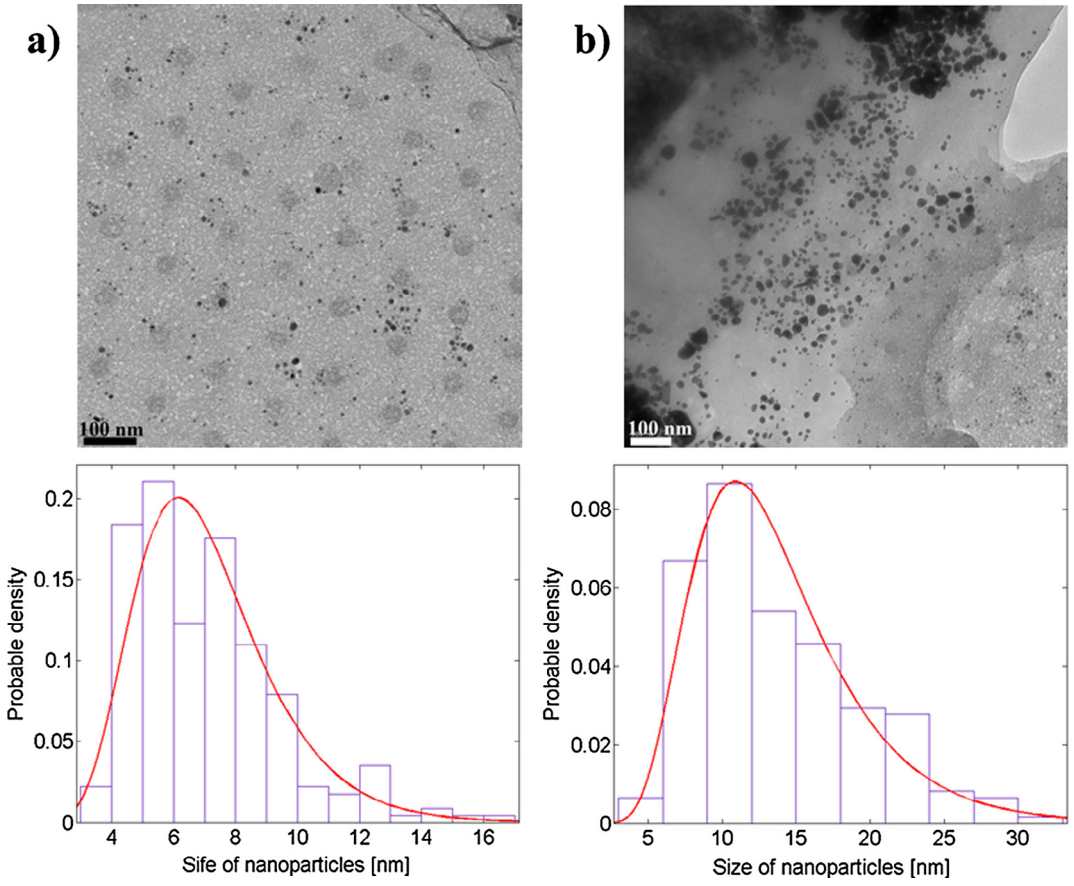

Fig. 5 TEM micrographs: (a) AuNPs on the surface of MK scales with particle size distribution histogram (below), (b) AuNPs around cellular debris stabilized in the external polymeric substances and particle size distribution histogram.

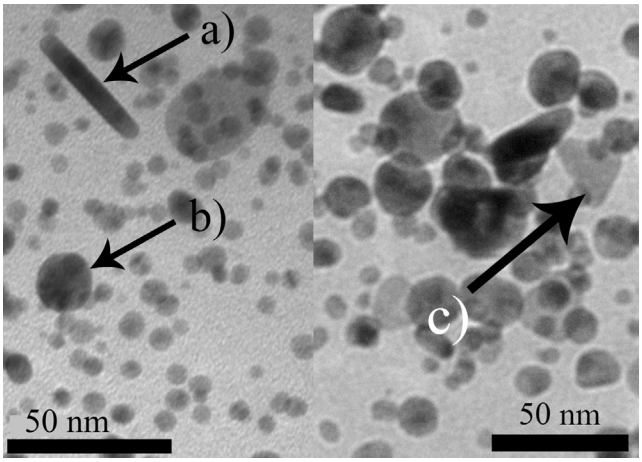

Fig. 6 Various morphological types of AuNPs biosynthesized by a chrysophyte siliceous alga *Mallomonas kalinae*: (a) rod-shaped, (b) spherical, (c) triangular.

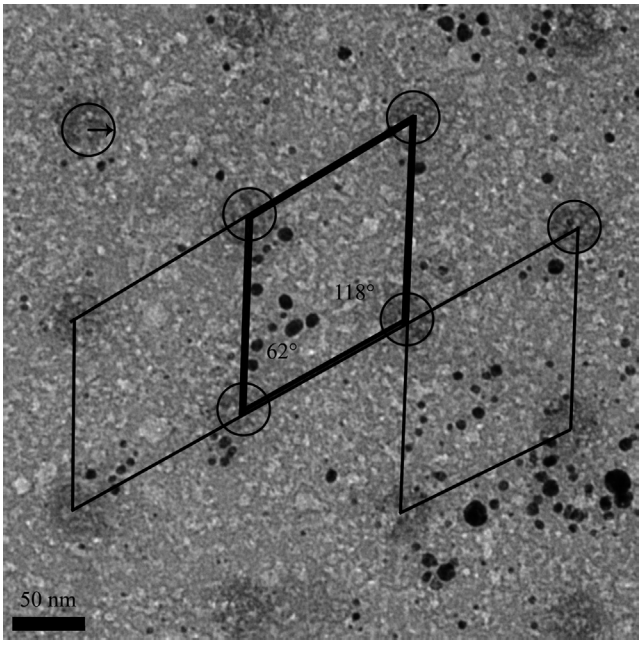

Fig. 7 Surface of MK silica scale with a system of pores, which were homogeneously distributed in a rhombohedral motive and designed in an extremely symmetric network on which the AuNPs were distributed (scale bar 50 nm).

region. After the biosynthesis, the band corresponding to C═O was shifted toward the lower wave numbers (from 1733 to 1719 cm^{-1}), on the contrary band 1045 cm^{-1} was shifted to the higher wave numbers (1062 cm^{-1}). The carbonyl group shift may be caused by the presence of biomolecules or their residues, which could have a strong ability to reduce and stabilize AuNPs (Abdel-Raouf et al., 2017; Mubarak Ali et al., 2013). Several bands disappeared from the MK–Au spectrum (1409, 1315, 590 cm^{-1}), which probably corresponds with the redox changes in the system after the bioreduction of AuNPs. Moreover, there was an interaction of AuNPs with biosilica as well. Shifting of the band at 1062 cm^{-1} (Si—O—Si) and occurrence of the band at 961 cm^{-1} (Si—O) point to the interaction of AuNPs with the surface of biosilica. O—H groups on the biosilica surface may be responsible for the biosynthesis of AuNPs (Mubarak Ali et al., 2013; Schröfel et al., 2011).

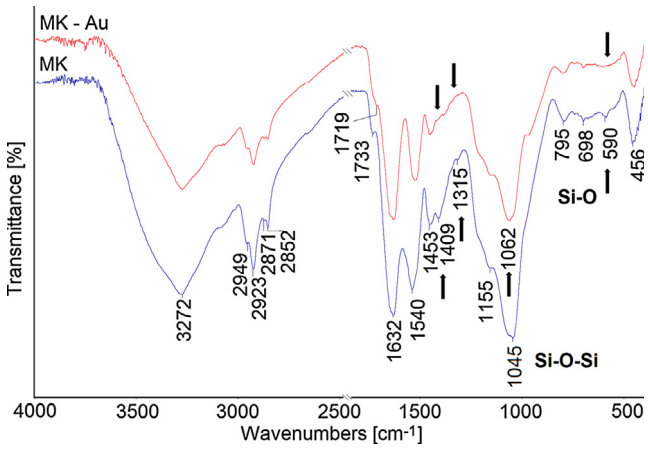

Fig. 8 FTIR spectra of pure MK cells and MK cells with AuNPs.

Initial dominant geochemical distribution of element speciations in the culture medium DY-V based on VM modeling are presented in Table 2. One of the important inorganic compounds in the system is H_4SiO_4 which is biologically transformed into the biosilica of MK cells. This result corresponds with FTIR analysis (Fig. 8).

Different bonds energy may occur in the biosilica system (Cölfen and Mann, 2003) . Klefenz et al. described Van der Wall's and repulsive bonds (Klefenz, 2004). Sumper and Kroger mentioned the existence of Si-O-Si and Si-OH bonds with active cations and anions, which supports the stability and integrity of nano- and mesoporous silica (Sumper and Kroger, 2004) and the formation of siloxane bonds (Ruiz-Hitzky et al., 2011; Schroder et al., 2008).

In our experiments, it was shown that the formation of AuNPs was caused not only by a response to the toxic effect of gold ions presented in the precursor. The strong interaction of the above-described types of bonds with gold ions may play a role in the nanoparticles biosynthesis as well. Bonds interactions on the biosilica system might be responsible for the rapid energy changes supporting the fast formation of AuNPs. In the solution, extracellular polymeric substances (EPS) are released by the MK cells. These EPS are diffused into the surrounding environment and act as a reducing agent. Generally, both the released EPS and the functional biosilica groups such as -OH groups are able to reduce Au^{3+} ions (Schroder et al., 2008; Sumper and Kroger, 2004).

The difference in the size of AuNPs (Fig. 5) is likely caused by the fact that in the close proximity of silica scales, more 3 D limitation exists than in the solution. Due to its 3 D structure, porosity and surface area; siliceous algae provide a high binding capacity environment with active reduction places and serve as a carrier for anchoring, stabilization, and functionalization of AuNPs. Moreover, the biosilica is known for its good chemical inertness (under conditions with high salinity and pH 2–7) and mechanical resistance (with high Young's modulus of tensile strength) (Gordon et al., 2009; Sumper and Kroger, 2004). With regard to a potential application in

Table 2 The geochemical distribution of element speciations in the culture medium DY-V designed in the Visual Minteq program for neutral pH.[a]

Element	Speciation	Element	Speciation	Element	Speciation
Ca^{2+}	Ca^{2+}	K^+	K^+	SO_4^{2-}	$MgSO_4$ (aq)
	$CaCl^+$		KCl (aq)		$CaSO_4$ (aq)
	$CaSO_4$(aq)		KNO_3 (aq)		$NaSO_4^-$
	$CaHCO_3^+$	Fe^{3+}	$FeEDTA^-$	CO_3^{2-}	H_2CO_3 (aq)
Mg^{2+}	Mg^{2+}	Cl^-	Cl^-	NO_3^-	NO_3^-
	$MgCl^+$		$CaCl^+$		$CaNO_3^+$
	$MgSO_4$ (aq)		$MgCl^+$	EDTA	$FeEDTA^-$
Na^+	Na^+		NaCl (aq)	H_4SiO_4	H_4SiO_4
	NaCl (aq)	SO_4^{2-}	SO_4^{2-}		

[a] According to the calculations in the VM program all element speciations exist in aqueous form and do not have a tendency to participate in other sorption and precipitation processes.

heterogeneous catalysis, it is advantageous that the biosilica structures of MK cells serve as a carrier of as-prepared nanoparticles (Gordon et al., 2009; Sumper and Kroger, 2004).

3.3. Catalytic activity of biosilica-nanogold composite and biosilica in GD degradation

The catalytic activity of two systems (i) MK-biosilica scales and (ii) MK-biosilica scales with AuNPs was compared with the control experiments of GD hydrolysis performed in demineralized water. Using the ICP-AES method, it was found that – after the biosynthesis – the total content of gold in the solution was 182 mg L^{-1} ± 19 mg L^{-1}. The results of biosilica-nanogold composite activity definitely proved a catalytic effect of nanogold on the GD disintegration (Fig. 9, matrices M3 and M6).

It is evident that in M3 the degradation of GD proceeds much faster than in demineralized water (M1, M4) or in an environment with pure MK cells (M2). The catalytic activity of AuNPs was also successfully verified by applying the nanoparticles in the mixture M6 with a higher concentration of GD. Fig. 9a also shows some catalytic activity of MK biosilica scales in the matrix M2. In the matrix with stronger concentrations of GD (M5, Fig. 9b), the catalytic effect of biosilica did, however, not manifest and control hydrolysis proceeded more efficiently.

The residual content of GD was 3.8% (M3) and 3.5% (M6) for both initial concentrations of GD (68 and 340 μg mL^{-1}, respectively) after 48 h of testing when the reaction was catalyzed by the biosilica-nanogold composite. In the case of GD degradation using pure MK biosilica, the concentration of GD decreased to 41% (M2) and 74.7% (M5) after 48 h of testing. In the control hydrolysis experiments, the concentrations of GD were 81.5% (M1) and 44.7% (M4) after the same time period.

The kinetic curves (Fig. 9), represent the rate of soman degradation for both concentrations by biosilica-nanogold composite and pure MK cells in comparison with spontaneous hydrolysis. The rate constants for spontaneous hydrolytic reaction were found to be 0.0052 h^{-1} and 0.0147 h^{-1} for lower and higher soman concentration. After the addition of pure MK cells, the rate constants were determined to be 0.0175 h^{-1} and 0.0055 h^{-1}. In the case of biosilica-nanogold composite, the rate constants for the degradation of soman were 0.0659 h^{-1} and 0.0621 h^{-1}. As shown in Fig. 9, soman was almost completely degraded within 48 h in the presence of biosilica-nanogold composite. The rate constants for the reaction of soman with AuNPs were approximately 12 and 4 times higher than for spontaneous hydrolysis. In the case of pure MK cells, the rate constants were 4 and 11 times lower than the reaction with biosilica-nanogold composite.

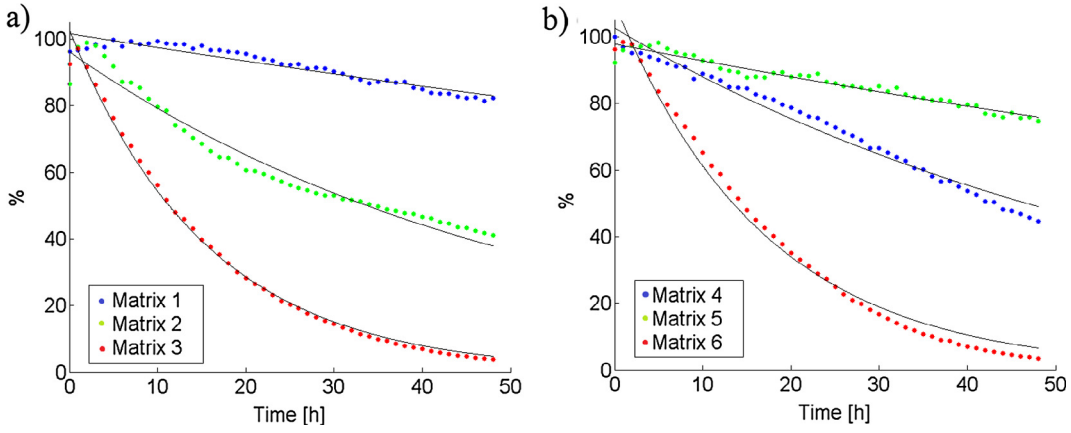

Fig. 9 Concentrations of GD in time during catalytic degradation with biosilica-nanogold composite (M3, M6) compared to control experiments with pure MK biosilica scales (M2, M5) and demineralized water (M1, M4).

Using our activated biosilica-nanogold material, we suppose at least three types of catalytic effects of soman degradation which are further described in detail. The first and probably the most dominant is that one resulting from the properties of nanogold. The catalytic activity of AuNPs depends on various parameters such as size and shape effects. In this study, the average size of AuNPs was found to be about 10 nm. The high catalytic activity of AuNPs is related to quantum-size effects generated by electrons confined within a small volume. Moreover, three morphological types (spherical, triangular and rod-shaped NPs) of biosynthesized crystalline AuNPs can influence hydrolysis of soman, due to both its shape-reactivity and selectivity (Cuenya, 2010). Generally, the literature (Kim et al., 2011) states that more basic environment shifts the equilibrium of the reaction to the degradation products. However, the catalytic effect of bionanogold was confirmed also in an acidic environment compared to control experiments, when the hydrolysis proceeded in, approximately, neutral pH.

Secondly, the role of the biosilica substrate of alga *Mallomonas kalinae* can help enhance the catalytic performance of AuNPs. This system is specific by location of active functional hydroxyl groups on its surface and may also participate in organophosphates degradation. Degradation experiments with a lower concentration of GD (68 μg mL^{-1}) showed catalytic activity of pure MK cells (M2, Fig. 9a). Meso- and nanoporous biosilica are interesting materials with bio-hybrid properties (Gordon et al., 2009; Ruiz-Hitzky et al., 2011). The active participation of mesoporous silica on diethyl cyanophosphonate (a tabun surrogate) degradation was observed e.g. by Candel (Candel et al., 2015). Regarding the aforementioned facts, we can assume that, in the mixture of MK cells and AuNPs, the catalytic effect is combined (synergistic effect).

The concentration of nerve poison in the reaction mixture most likely plays an important role, because the degradation of GD only with pure MK cells is not apparent when a higher concentration of GD is applied (Fig. 9b). A higher concentration of soman in the matrix (M5) may inhibit the catalytic activity of biosilica as well as enzymatic activity (which is discussed below) - and it may also contribute to the degradation of organophosphates. Furthermore, the results showed that the hydrolysis in the matrix with more concentrated GD (M4) proceeded better than in the matrix with a lower concentration of GD (M1). Reducing the concentration of soman to 68 μg mL^{-1} may result in an excess of water. This means that the equilibrium reaction may be disrupted and the reaction will proceed in favor of the reactants (Guldberg-Waag law).

Finally, various biomolecules (e.g. enzymes) released after the contact of the gold precursor and MK cells are involved in bioreduction of catalytically active nanogold particles as well as in the degradation of nerve poison. This hypothesis would need a further in-depth understanding of the particular bioreduction mechanism; however, there are a number of works that use enzymes for the degradation of CW agents and degradation activity of enzymes on organophosphates is currently being studied intensively. Polymeric substances released from MK cells during the biosynthesis may support GD degradation as well. For instance, a preferred strategy for preventing intoxication is catalytic scavenging by paraoxonase 1 that hydrolyzes NA before they reach their targets (Goldsmith et al., 2012). Another work was focused on the degradation of the nerve gas using enzymes of microbial prolidases (Iyer and Iken, 2015). Amitai et al. described experiments of degradation of NA and other CWA by enzymatic haloperoxidation (Amitai et al., 2003). Borkar and colleagues prepared bionanoconjugate-based composites with organophosphorus hydrolase for decontamination of NA (Borkar et al., 2010).

Bis (1,2,2-trimethyl propyl) ester of methyl phosphonic acid (CAS: 7040-58-6), 2-chloro-2,3-dimethyl butane (CAS: 594-57-0) and 1-chloro-3,3-dimethylbutane (CAS: 2855-08-5) were detected as degradation products of GD (Scheme 1). Degradation products of GD could interact with a wide spectrum of inorganic and organic (biohybrid) forms existing in the DY-V medium (Table 2). This is well documented by VM modeling, which confirmed the presence of dissolved chloride anion in the reaction mixture. Chlorine that occurs in the gold precursor $HAuCl_4$ (0.1 M) or in the DY-V medium can thus be responsible for further chlorine interaction with and incorporation into the structure of degradation products.

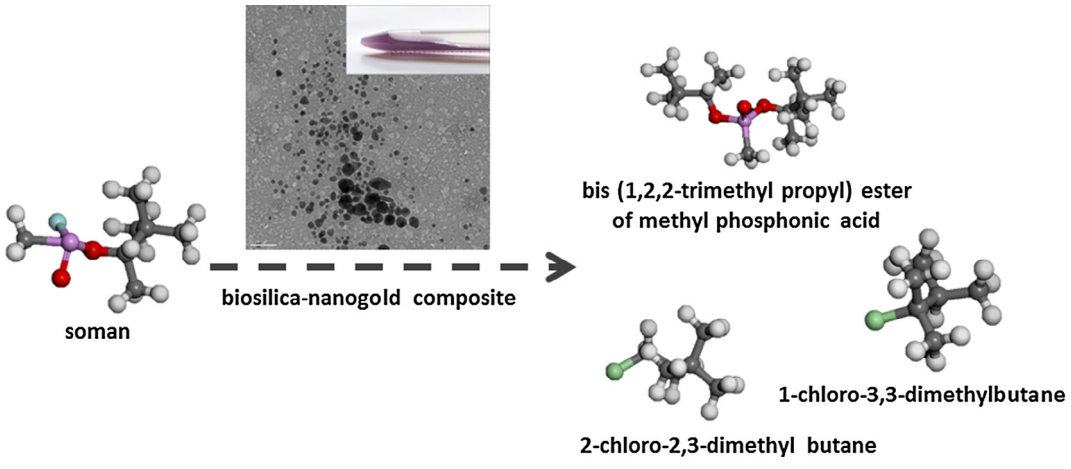

Scheme 1 Products of soman degradation catalyzed by biosilica-nanogold composite.

3.4. Future prospects in nanocatalysts preparation via biosynthesis

The main advantage of biosilica-nanogold composite preparation via biosynthesis is easier preparation compared to conventional chemical and physical protocols (Ahmed et al., 2016; Manivasagan and Kim, 2015) . Moreover, the catalytic activity of composite was observed under laboratory conditions (day/night) without the use of special radiation. Taking into account that the almost total conversion of GD is observed after 48 h, the biosilica-nanogold composite cannot be used for immediate degradation of NA. However, this nanomaterial is environmentally more inert in contrast to the chemicals commonly used to break down the CWA, which are mostly toxic and corrosive. AuNPs do not show considerable toxic effects on living organisms (Bommavaram et al., 2013). This may be advantageous for using of bionanocomposite in a catalytic decontamination of valuable materials and equipment (instruments, tools, etc.), which must remain undamaged. In the case of stabilizing the nanocatalyst on a solid carrier (silica, activated coal, clay minerals, etc.), the usefulness of such catalysts is much higher, e.g. for decontamination of fabrics, surfaces from the secondary contamination, or for sensitive detection purposes (indication of degradation products' presence).

Different biosynthesis protocols may lead to a large scale of morphologies and sizes of AuNPs. Therefore, further research will be focused on biosynthesis optimization to achieve stable AuNPs under 10 nm in order to enhance their catalytic activity. The unique catalytic properties of AuNPs may be further enhanced by combining the nanogold with other (nano) materials, for example, TiO_2 (Alvaro et al., 2010; Panayotov and Morris, 2008). One of the candidates for preparation of bimetallic nanomaterials may be ZrO_2, which is cheaper than gold, can be prepared biosynthetically and also ZrO_2 nanoparticles dispose of catalytic properties (Gole et al., 2006). A wide range of organisms which are readily available (or even secondary raw biomass) may also be exploited for biosynthesis.

4. Conclusions

Currently, the advances in research of biosynthesis are accelerated by simplicity of the nanoparticles preparation in comparison with the conventional chemical and physical protocols. Low cost and low environmental burden also attract more and more attention to these methods of nanomaterials preparation. Our results underline the new approach of nanogold biosynthesis using siliceous alga called *Mallomonas kalinae*. Functional and catalytically active bionanocomposite was prepared *in vitro* using eco-friendly, bottom-up approach. In one simple step, AuNPs were formed, stabilized and anchored on the biosilica surface producing a composite material with potential in heterogeneous catalysis. The catalytic activity of bionanogold was further verified in the degradation of the nerve poison soman. A significant catalytic effect of AuNPs was observed in the degradation of soman in comparison with control experiments. However, it may be assumed that the presence of biosilica and biomolecules released from MK cells affects the disintegration of nerve poison as well. This research presents interdisciplinary connections in the area of bio- and nanotechnology focusing on the application potential of materials prepared using green chemistry protocols.

Acknowledgments

We would also like to thank Oldřich Motyka and Jay Davis for a thorough correction of the English language and Kateřina Mamulová Kutláková for carrying X-ray diffraction analysis and interpretation of results.

Funding

This work was supported by the SGS projects of Czech Republic [SP2015/65 and SP2016/72], project VG of Ministry of Interior of Czech Republic [20102014049], the Ministry of Education, Youth and Sports of CR within the LQ1604 National Sustainability Program II (Project BIOCEV-FAR) and by the project "BIOCEV" [CZ.1.05/1.1.00/02.0109], and by Scientific Grant Agency of the Ministry of Education of Slovak Republic and the Slovak Academy of Sciences under the contracts No. VEGA 1/0164/17, and KEGA 014SPU-4/2016.

References

Abdel-Raouf, N., Al-Enazi, N.M., Ibraheem, I.B.M., 2017. Green biosynthesis of gold nanoparticles using Galaxaura elongata and characterization of their antibacterial activity. Arab. J. Chem. 10, S3029–S3039. http://dx.doi.org/10.1016/j.arabjc.2013.11.044.

Ahmed, S., Annu, Ikram, S., S., S.Y., 2016. Biosynthesis of gold nanoparticles: a green approach. J. Photochem. Photobiol. B Biol. 161, 141–153. doi: http://dx.doi.org/10.1016/j.jphotobiol.2016.04.034.

Alvaro, M., Cojocaru, B., Ismail, A.A., Petrea, N., Ferrer, B., Harraz, F.A., Parvulescu, V.I., Garcia, H., 2010. Visible-light photocatalytic activity of gold nanoparticles supported on template-synthesized mesoporous titania for the decontamination of the chemical warfare agent Soman. Appl. Catal. B Environ. 99, 191–197. http://dx.doi.org/10.1016/j.apcatb.2010.06.019.

Amitai, G., Adani, R., Hershkovitz, M., Bel, P., Rabinovitz, I., Meshulam, H., 2003. Degradation of VX and sulfur mustard by enzymatic haloperoxidation. J. Appl. Toxicol. 23, 225–233. http://dx.doi.org/10.1002/jat.911.

Andersen, R.A., Morton, S.L., Sexton, J.P., 1997. Provasoli-Guillard national center for culture of marine phytoplankton 1997 list of strains. J. Phycol. 33, 1–75. http://dx.doi.org/10.1111/j.0022-3646.1997.00001.x.

Bommavaram, M., Korivi, M., Borelli, D.P.R., Pabbadhi, J.D., Nannepaga, J.S., 2013. Bacopa monniera stabilized gold nanoparticles (BmGNPs) alleviated the oxidative stress induced by aluminum in albino mice. Drug Invent. Today 5, 113–118. http://dx.doi.org/10.1016/j.dit.2013.05.001.

Borkar, I.V., Dinu, C.Z., Zhu, G., Kane, R.S., Dordick, J.S., 2010. Bionanoconjugate-based composites for decontamination of nerve agents. Biotechnol. Prog. 26, 1622–1628. http://dx.doi.org/10.1002/btpr.498.

Candel, I., Marcos, M.D., Martínez-Máñez, R., Sancenón, F., Costero, A.M., Parra, M., Gil, S., Guillem, C., Pérez-Plá, F., Amorós, P., 2015. Hydrolysis of DCNP (a Tabun mimic) catalysed by mesoporous silica nanoparticles. Microporous Mesoporous Mater. 217, 30–38. http://dx.doi.org/10.1016/j.micromeso.2015.05.041.

Cölfen, H., Mann, S., 2003. Higher-order organization by mesoscale self-assembly and transformation of hybrid nanostructures. Angew. Chemie Int. Ed. 42, 2350–2365. http://dx.doi.org/10.1002/anie.200200562.

Corti, R.H.C., 2010. Gold: Science and Applications. CRC Press, Boca Raton, FL.

Cuenya, B.R., 2010. Synthesis and catalytic properties of metal nanoparticles: Size, shape, support, composition, and oxidation state effects. Thin Solid Films 518, 3127–3150. http://dx.doi.org/10.1016/j.tsf.2010.01.018.

Goldsmith, M., Ashani, Y., Simo, Y., Ben-David, M., Leader, H., Silman, I., Sussman, J.L., Tawfik, D.S., 2012. Evolved stereoselective hydrolases for broad-spectrum G-type nerve agent detoxification. Chem. Biol. 19, 456–466. http://dx.doi.org/10.1016/j.chembiol.2012.01.017.

Gole, J.L., Prokes, S.M., Stout, J.D., Glembocki, O.J., Yang, R., 2006. Unique properties of selectively formed zirconia nanostructures. Adv. Mater. 18, 664–667. http://dx.doi.org/10.1002/adma.200500769.

Gopinath, V., Priyadarshini, S., MubarakAli, D., Loke, M.F., Thajuddin, N., Alharbi, N.S., Yadavalli, T., Alagiri, M., Vadivelu, J., 2019. Anti-Helicobacter pylori, cytotoxicity and catalytic activity of biosynthesized gold nanoparticles: multifaceted application. Arab. J. Chem. 12 (1), 33–40. http://dx.doi.org/10.1016/j.arabjc.2016.02.005.

Gordon, R., Losic, D., Tiffany, M.A., Nagy, S.S., Sterrenburg, F.A.S., 2009. The Glass Menagerie: diatoms for novel applications in nanotechnology. Trends Biotechnol. 27, 116–127. http://dx.doi.org/10.1016/j.tibtech.2008.11.003.

Gupta, R.C., 2009. Handbook of Toxicology of Chemical Warfare Agents. Academic Press, London.

Iyer, R., Iken, B., 2015. Protein engineering of representative hydrolytic enzymes for remediation of organophosphates. Biochem. Eng. J. 94, 134–144. http://dx.doi.org/10.1016/j.bej.2014.11.010.

Romano Jr., J.A., Salem, H., Lukey, B.J., 2008. Chemical warfare agents: chemistry, pharmacology, toxicology, and therapeutics. CRC Press, Boca Raton.

Jablonski, D., 1990. On Biomineralization. Heinz A. Lowenstam, Stephen Weiner. J. Geol. 98, 977. http://dx.doi.org/10.1086/629466.

Janoš, P., Kuráň, P., Pilařová, V., Trögl, J., Šťastný, M., Pelant, O., Henych, J., Bakardjieva, S., Životský, O., Kormunda, M., Mazanec, K., Skoumal, M., 2015. Magnetically separable reactive sorbent based on the CeO_2/γ-Fe_2O_3 composite and its utilization for rapid degradation of the organophosphate pesticide parathion methyl and certain nerve agents. Chem. Eng. J. 262, 747–755. http://dx.doi.org/10.1016/j.cej.2014.10.016.

Karpouzas, D.G., Singh, B.K., 2006. Microbial Degradation of Organophosphorus Xenobiotics: Metabolic Pathways and Molecular Basis. Adv. Microb. Physiol. 51, 119–225. http://dx.doi.org/10.1016/S0065-2911(06)51003-3.

Khan, A., Rashid, R., Murtaza, G., Zahra, a., 2014. Gold nanoparticles: synthesis and applications in drug delivery. Trop. J. Pharm. Res. 13, 1169–1177. http://dx.doi.org/10.1055/s-2006-944219.

Kim, K., Tsay, O.G., Atwood, D.A., Churchill, D.G., 2011. Destruction and detection of chemical warfare agents. Chem. Rev. 111, 5345–5403. http://dx.doi.org/10.1021/cr100193y.

Klefenz, H., 2004. Nanobiotechnology: from molecules to systems. Eng. Life Sci. 4, 211–218. http://dx.doi.org/10.1002/elsc.200402090.

Kolenčík, M., Urík, M., Čaplovičová, M., 2014. Unexpected formation of Ag_2SO_4 microparticles from Ag_2S nanoparticles synthesised using poplar leaf extract. Environ. Chem. Lett. 12, 551–556. http://dx.doi.org/10.1007/s10311-014-0484-0.

Komano, A., Hirakawa, T., Sato, K., Kishi, S., Nishimoto, C.K., Mera, N., Kugishima, M., Sano, T., Negishi, N., Ichinose, H., Seto, Y., Takeuchi, K., 2013. Titanium dioxide photocatalytic decomposition of ethyl-S-dimethylaminoethyl methylphosphonothiolate (VX) in aqueous phase. Appl. Catal. B Environ. 134, 19–25. http://dx.doi.org/10.1016/j.apcatb.2012.12.036.

Makarska-Bialokoz, M., Kaczor, A.A., 2014. Computational analysis of chlorophyll structure and UV-Vis spectra: a student research project on the spectroscopy of natural complexes. Spectrosc. Lett. 47, 147–152. http://dx.doi.org/10.1080/00387010.2013.781038.

Manivasagan, P., Kim, S., 2015. Biosynthesis of nanoparticles using marine algae: a review. Mar. Algae Extr. Process. Prod. Appl. 30, 295–304. http://dx.doi.org/10.1002/9783527679577.ch17.

MubarakAli, D., Arunkumar, J., Nag, K.H., SheikSyedIshack, K.A., Baldev, E., Pandiaraj, D., Thajuddin, N., 2013. Gold nanoparticles from Pro and eukaryotic photosynthetic microorganisms—comparative studies on synthesis and its application on biolabelling. Coll. Surf. B Biointerf. 103, 166–173. http://dx.doi.org/10.1016/j.colsurfb.2012.10.014.

Němec, V.Š.V.H.S.B.N.M.M.M.F.O.T., 2010. Zirconium doped nanodispersed oxides of Fe, Al and Zn for destruction of warfare agents. Mater. Charact. 61, 1080–1088. http://dx.doi.org/10.1016/j.matchar.2010.06.021.

Oliveira, R.C., Hammer, P., Guibal, E., Taulemesse, J.-M., Garcia, O., 2014. Characterization of metal–biomass interactions in the lanthanum(III) biosorption on Sargassum sp. using SEM/EDX, FTIR, and XPS: Preliminary studies. Chem. Eng. J. 239, 381–391. http://dx.doi.org/10.1016/j.cej.2013.11.042.

Organization for the prohibition of chemical weapons [WWW Document], 2014. Conv. Prohib. Dev. Prod. Stock. Use Chem. Weapons their Destr. < https://www.opcw.org/chemical-weapons-convention/ > (accessed 7.18.17).

Panayotov, D.A., Morris, J.R., 2008. Catalytic degradation of a chemical warfare agent simulant: reaction mechanisms on TiO_2-supported au nanoparticles. J. Phys. Chem. C 112, 7496–7502. http://dx.doi.org/10.1021/jp7118668.

Ruiz-Hitzky, E., Aranda, P., Darder, M., Ogawa, M., 2011. Hybrid and biohybrid silicate based materials: molecular vs. block-assembling bottom-up processes. Chem. Soc. Rev. 40, 801–828. http://dx.doi.org/10.1039/C0CS00052C.

Schroder, H.C., Wang, X., Tremel, W., Ushijima, H., Muller, W.E.G., 2008. Biofabrication of biosilica-glass by living organisms. Nat. Prod. Rep. 25, 455–474. http://dx.doi.org/10.1039/B612515H.

Schröfel, A., Kratošová, G., Bohunická, M., Dobročka, E., Vávra, I., 2011. Biosynthesis of gold nanoparticles using diatoms–silica-gold and EPS-gold bionanocomposite formation. J. Nanoparticle Res. 13, 3207–3216. http://dx.doi.org/10.1007/s11051-011-0221-6.

Schröfel, A., Kratošová, G., Šafařík, I., Šafaříková, M., Raška, I., Shor, L.M., 2014. Applications of biosynthesized metallic nanoparticles – a review. Acta Biomater. 10, 4023–4042. http://dx.doi.org/10.1016/j.actbio.2014.05.022.

Sumper, M., Kroger, N., 2004. Silica formation in diatoms: the function of long-chain polyamines and silaffins. J. Mater. Chem. 14, 2059–2065. http://dx.doi.org/10.1039/B401028K.

Sweeney, R.Y., Mao, C., Gao, X., Burt, J.L., Belcher, A.M., Georgiou, G., Iverson, B.L., 2004. Bacterial biosynthesis of cadmium sulfide nanocrystals. Chem. Biol. 11, 1553–1559. http://dx.doi.org/10.1016/j.chembiol.2004.08.022.

Vágó, A., Szakacs, G., Sáfrán, G., Horvath, R., Pécz, B., Lagzi, I., 2016. One-step green synthesis of gold nanoparticles by mesophilic filamentous fungi. Chem. Phys. Lett. 645, 1–4. http://dx.doi.org/10.1016/j.cplett.2015.12.019.

Zboril, R., Andrle, M., Oplustil, F., Machala, L., Tucek, J., Filip, J., Marusak, Z., Sharma, V.K., 2012. Treatment of chemical warfare agents by zero-valent iron nanoparticles and ferrate(VI)/(III) composite. J. Hazard. Mater. 211, 126–130. http://dx.doi.org/10.1016/j.jhazmat.2011.10.094.

Zhang, X., Qu, Y., Shen, W., Wang, J., Li, H., Zhang, Z., Li, S., Zhou, J., 2016. Biogenic synthesis of gold nanoparticles by yeast Magnusiomyces ingens LH-F1 for catalytic reduction of nitrophenols. Coll. Surf. A Physicochem. Eng. Asp. 497, 280–285. http://dx.doi.org/10.1016/j.colsurfa.2016.02.033.

Zhang, Y., Jiang, J., Chen, M., 2008. MINTEQ modeling for evaluating the leaching behavior of heavy metals in MSWI fly ash. J. Environ. Sci. 20, 1398–1402. http://dx.doi.org/10.1016/S1001-0742(08)62239-1.